Homeostatic control of spontaneous activity in the developing auditory system

Travis A. Babola[1], **Sally Li**[1], **Alexandra Gribizis**[2], **Brian J. Lee**[1], **John B. Issa**[3], **Han Chin Wang**[1], **Michael C. Crair**[2], and **Dwight E. Bergles**[*,1,4,5]

[1]The Solomon Snyder Department of Neuroscience, Johns Hopkins University, Baltimore, Maryland 21205, USA

[2]Department of Neurobiology, Yale University School of Medicine, New Haven, Connecticut 06510, USA

[3]Department of Biomedical Engineering, Johns Hopkins University, Baltimore, Maryland 21218, USA

[4]Department of Otolaryngology Head and Neck Surgery, Johns Hopkins University, Baltimore, Maryland 21287, USA

[5]Johns Hopkins University Kavli Neuroscience Discovery Institute, Baltimore, Maryland, 21205

SUMMARY

Neurons in the developing auditory system exhibit spontaneous bursts of activity before hearing onset. How this intrinsically generated activity influences development remains uncertain, because few mechanistic studies have been performed *in vivo.* We show using macroscopic calcium imaging in unanesthetized mice that neurons responsible for processing similar frequencies of sound exhibit highly synchronized activity throughout the auditory system during this critical phase of development. Spontaneous activity normally requires synaptic excitation of spiral ganglion neurons (SGNs). Unexpectedly, tonotopic spontaneous activity was preserved in a mouse model of deafness in which glutamate release from hair cells is abolished. SGNs in these mice exhibited enhanced excitability, enabling direct neuronal excitation by supporting cell-induced potassium transients. These results indicate that homeostatic mechanisms maintain spontaneous activity in the pre-hearing period, with significant implications for both circuit development and therapeutic approaches aimed at treating congenital forms of deafness arising through mutations in key sensory transduction components.

[*]Corresponding author. Lead Contact/Correspondence: Dwight E. Bergles, PhD, Solomon H. Snyder Department of Neuroscience, Johns Hopkins University School of Medicine, 725 N. Wolfe Street, Baltimore, MD 21205, USA, P:410-955-6939, dbergles@jhmi.edu.
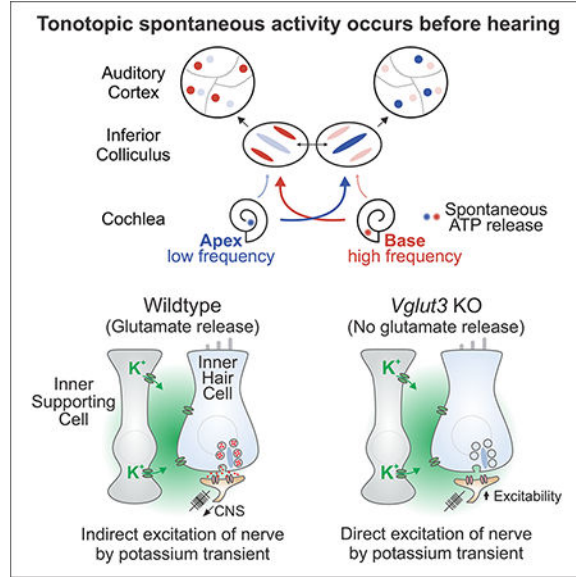
DECLARATION OF INTERESTS

The authors declare no competing financial interests.

Graphical Abstract

Tonotopic spontaneous activity occurs before hearing

INTRODUCTION

Information about the external world is acquired by sensory organs, which extract component features of signals generated within the environment and convey this deconstructed information to higher centers within the brain. In the auditory system, sound frequency is encoded through excitation of different hair cells, due to the exquisite partitioning of sound-induced vibrations along the length of the organ of Corti. This tonotopic segregation is preserved as signals progress to first-order spiral ganglion neurons (SGNs) in the cochlea and then through auditory centers in the brain, creating a spatial map of the frequency components of complex sounds (Schreiner and Winer, 2005). These precise neural pathways are established through a combination of genetically pre-programmed events, involving guidance of axonal projections to appropriate recipient neurons segregated along isofrequency lines (Allen-Sharpley and Cramer, 2012), and activity-dependent processes that promote maturation of neurons and refinement of their connections during early life (Clause et al., 2014, 2017). Remarkably, this period of activity-dependent modification begins prior to the onset of hearing, with neurons along these pathways exhibiting highly stereotyped bursts of action potentials during this crucial developmental period (Sonntag et al., 2009; Tritsch et al., 2010a). Although detailed information has been obtained about the patterns of activity exhibited by individual neurons using electrophysiological methods (Crins et al., 2011; Jones et al., 2007; Sonntag et al., 2009), little is known about the relationship between this activity and future tonotopic zones, the degree of correlation between neurons in different auditory centers or the interaction between this peripherally generated activity to other forms of spontaneous activity within the brain.

Spontaneous activity in the auditory system is conserved across species (Wang and Bergles, 2014) and originates in the developing cochlea, as removal of the cochlea or application of

TTX to the oval window results in cessation of burst firing in the CNS (Lippe, 1994; Tritsch et al., 2010b). Previous studies suggest that the primary generator of this activity in the period just before hearing onset is a group of inner supporting cells that form a transient epithelium known as Kölliker's organ (or Greater Epithelial Ridge, GER) that is located adjacent to inner hair cells (IHCs) (Tritsch et al., 2007). Individual supporting cells located near inner hair cells periodically release ATP, which initiates a cascade of events culminating in the release of potassium. These local increases in potassium within the organ of Corti depolarize groups of neighboring inner hair cells (IHCs), inducing calcium spikes, glutamate release and eventual excitation of SGNs (Tritsch et al., 2010b; Wang et al., 2015). Although stochastic and highly variable in both location and magnitude, this mechanism for inducing spontaneous activity reliably induces co-activation of neurons that will ultimately encode similar frequencies of sound, providing a means for Hebbian-based reinforcement of synapses and cellular maturation within isofrequency zones. While the mechanisms that initiate spontaneous activity have been explored extensively *in vitro* (Clause et al., 2014; Johnson et al., 2011, 2012, 2017; Tritsch et al., 2007; Zhang-Hooks et al., 2016), a system-wide analysis of spontaneous activity *in vivo* in unanesthetized mice has so far not been achieved. This has prevented analysis of the propagation and coordination of activity in distinct auditory centers, information necessary to understand how spontaneous activity patterns regulate maturation of neuronal connectivity throughout the auditory pathway.

Here, we performed *in vivo* imaging in awake transgenic mice that express genetically-encoded calcium indicators to define the spatial and temporal patterns of neural activity in auditory centers before the onset of hearing. Our studies reveal that groups of neurons aligned to the future tonotopic axis in the inferior colliculus (IC) exhibit transient bouts of highly correlated activity. This activity originated in the cochlea and traversed through brainstem and midbrain auditory centers before reaching auditory cortex, indicating that neurons that will later process similar frequencies of sound are synchronized throughout the auditory pathway during this highly dynamic period of development. To determine how disruption of communication between IHCs and SGNs, a common cause of deafness, influences spontaneous activity patterns, we imaged neuronal activity in auditory centers from mice in which vesicular glutamate release from IHCs was abolished. Unexpectedly, discrete tonotopically-organized spontaneous events still occurred in the IC of these mice that was dependent on input from the cochlea. This preservation of activity was enabled through enhanced excitability of SGNs, which allowed these neurons to be directly excited by local potassium transients. The ability of SGNs to maintain spontaneous activity in the absence of IHC input may help preserve the auditory nerve by preventing neuronal apoptosis and promote maturation of at least some aspects of sound processing circuits in the brain, thereby improving the performance of cochlear implants and the outcome of therapies designed to correct mutations that lead to common inherited forms of deafness.

RESULTS

Central auditory neurons exhibit correlated activity aligned to the tonotopic axis.

Spontaneous activity initiated in the developing cochlea prior to hearing onset propagates to central auditory centers where it has the opportunity to influence the maturation of sound

processing circuits. To define the spatial and temporal pattern of activity that propagates through these nascent circuits, we used wide field epifluorescence microscopy (Ackman et al., 2012) to visualize calcium transients in the midbrain of *Snap25-T2A-GCaMP6s* mice (Madisen et al., 2015) (Figure 1A), which express the genetically-encoded calcium indicator GCaMP6s in all neurons (Figure S1). A cranial window was installed over the exposed inferior and superior colliculi (Figure 1B), which receive auditory and visual information, respectively, and time-lapse recordings were performed in awake (unanesthetized) mice prior to hearing onset (P7). Groups of neurons in both regions exhibited periodic calcium transients (increases in GCaMP6s fluorescence) lasting several seconds (Figure 1C), consistent with the intermittent bursts of action potentials generated by neurons in these regions at this age (Ackman et al., 2012; Tritsch et al., 2010); however, the spatial patterns of activity occurring in these two regions were distinct. As described previously (Ackman et al., 2012), neuronal activity in the superior colliculus (SC) propagated as waves that followed irregular trajectories, reflecting the pattern of retinal ganglion cell activity that occurs prior to eye opening. In contrast, neuronal activity in the inferior colliculus (IC) was confined to discrete, stationary bands oriented diagonally along the anterior-lateral to posterior-medial axis (Figure 1D and Movie S1). Events that occurred near the central region of the IC consisted of a single band, while events that engaged neurons flanking this region consisted of two bands. The spatial organization and timing of events were mirrored across both lobes of the IC (Figure S2A-I), but the amplitude of calcium transients exhibited strong lateral bias, with the lobe exhibiting the largest calcium increase varying from event to event (Figure 1E, F). In addition, although the average event amplitude and bilateral amplitude ratio (small side/large side) was similar between zones, the degree of lateral bias varied from event to event (Figure 1F, and S2F), indicating that bilateral representation of activity is not fixed.

Despite the lateral bias of each event, the average waveform of events was similar (Figure 1G), and over time, neurons throughout the IC exhibited similar activity (Figure 1C and S2G; see Figure 3B below). These periodic events within the IC were not induced by sound, as neither self-induced vocalizations nor exposure to loud sounds induced similar patterned activity at this age (Figure S3A-E). In addition, although animal movement occasionally elicited widespread neuronal activity in the midbrain and cortex, these movement-associated events were much less frequent than the overall rate of spontaneous activity in the IC (0.9 ± 0.2 vs 8.5 ± 0.5 transients per minute) (Figure S3G-J). The spatial patterning of spontaneous events appeared to correspond to the future tonotopic organization of IC (Barnstedt et al., 2015; Malmierca et al., 1995). Indeed, exposing hearing animals to tones of different frequencies mimicked the distinct spatial patterns observed before hearing onset (Figures 1H and 1I). A low frequency tone (3 kHz) activated neurons in single bands in both lobes of the IC, with greater fluorescence seen in the IC contralateral to the speaker. Higher frequency sounds elicited dual bands in each lobe of the IC, with activated zones moving progressively more lateral with increasing frequency. These findings indicate that neurons located in future isofrequency zones within the developing IC exhibit highly correlated firing prior to hearing onset.

To define the cellular origin of this correlated activity, we performed high resolution, two photon imaging within the dorsal aspect of the central nucleus of the IC (150 μm from the

pial surface) (Figure 2A). As suggested by the wide field imaging, neurons and the surrounding neuropil in this region exhibited large-scale correlated activity (Figure 2B and 2C). Pre-labeling astrocytes with the fluorescent dye SR101 (Nimmerjahn and Helmchen, 2012) revealed that fluorescence changes occurred in neuronal cell bodies and processes rather than in astrocytes (Figure 2B; Movie S2), as expected due to the neuronal specificity of the Snap25 promoter (Madisen et al., 2015). Groups of neurons within distinct spatial domains contributed to individual events, with highly correlated activity exhibited by neurons (and neuropil) along diagonal bands aligned to the tonotopic organization of the IC (Figure 2D and 2E). Together, these results indicate that groups of neurons in the IC that will ultimately process similar frequencies of sound exhibit robust, correlated activity prior to hearing onset. Studies in hearing animals indicate that sound detected by each ear is represented primarily in the contralateral IC (Hind et al., 1963), but that weak ipsilateral projections and collaterals between the lobes of the IC ensure bilateral representation (Coleman and Clerici, 1987; González Hernández et al., 1986), providing an explanation for the mirroring of spontaneous events across the IC (Figure 2F). Moreover, the periodic, tonotopic nature of this activity is consistent with prior studies indicating that occasional release of ATP by inner supporting cells within the cochlea is sufficient to induce correlated firing of groups of IHCs in discrete locations along the organ of Corti (Tritsch et al., 2007; Wang et al., 2015).

Spontaneous activity in the inferior colliculus originates in the cochlea

To assess the contribution of peripheral cochlear input to spontaneous activity in the IC, we performed cochlear ablations just prior to wide field imaging. In both naive mice and mice subjected to sham surgery, the largest spontaneous events alternated stochastically between lobes of the IC (in Figure 3A, the magnitude of fluorescence change for each event is indicated by the length of the horizontal bar, and degree of difference between the two lobes of the IC is indicated by the size of circle), achieving equally balanced activity over ~ 10 minutes (Figure 3A,B), in terms of location of largest event amplitude (Figure 3C) and the event frequency for each lobe (Figure 3D). If spontaneous activity in the IC arises from the cochlea, then unilateral cochlear removal should decimate activity in the IC contralateral to the ablation, due to the contralateral bias in flow of auditory information from the cochlea to the midbrain (Semple and Kitzes, 1985). Indeed, animals with unilateral cochlear ablation exhibited a profound bias towards the ipsilateral side, with nearly all calcium transients being larger, and the frequency of events greater, in the lobe ipsilateral to the ablation (Figure 3C-F). Removal of both cochleae nearly abolished activity in both lobes of the IC (Figure 3C,D,G), without altering waves in the SC (Figure S4), demonstrating that activity in central auditory centers is initiated within these peripheral sensory organs.

Spontaneous activity propagates from the IC to the auditory cortex

Auditory information is extensively processed through reciprocal connections between subcortical structures and the auditory cortex (Syka and Popelá , 1984; Yan and Suga, 1996), allowing sound information to be modulated by internal states (Francis et al., 2018; Kilgard and Merzenich, 1998). To determine if spontaneous activity originating in the cochlea propagates to the auditory cortex (AC) prior to hearing onset, we performed simultaneous wide field imaging of the midbrain and the posterior portion of the temporal

and occipital cortex in P7 *Snap25-T2A-GCaMP6s* mice, enabling simultaneous visualization of neuronal activity patterns in both auditory and visual centers (Figure 4A). Neurons in these regions of cortex exhibited robust, spontaneous activity at this age, characterized by transient increases in calcium by groups of neurons in complex spatio-temporal patterns (Movie S3). To assess whether any of this cortical activity was correlated with events occurring in the IC, we subjected movies to unbiased segmentation using the IC as a reference (see Methods). This analysis revealed that neurons within a discrete region of temporal cortex corresponding to the approximate future region of AC (RAS coordinates (mm): 5.07, −2.57, 2.29) exhibited correlated activity with IC neurons (yellow areas, Figure 4B). For a given correlated event, the amplitude of the fluorescence change was larger in AC than IC (Figure 4C and 4D), which may arise through higher levels of GCaMP6s in the cortex (Figure S1) and/or amplification of sensory information from the thalamus to the cortex (Murata and Colonnese, 2016). Although the majority of events in AC (80 ± 3%, n = 7 animals) were correlated with activity in IC, large-scale events synchronized across diverse regions of the cortex (e.g between AC and VC) were also observed (asterisks, Figure 4C) that were independent of activity in IC. Alignment of average waveforms for correlated IC:AC events revealed that they had a comparable time course (Figure 4E), but that events in AC were consistently delayed by ≤ 100 ms relative to IC, visible from the temporal shift in both the leading edge (Figure 4E) and peak (Figure 4F) of these events, suggesting that activity propagates from IC to AC. When a comparable correlation analysis was performed using spatial masks over VC and SC (Figure 4B), the correlation coefficient determined for IC:AC (r = 0.86 ± 0.01) was significantly higher than between IC and other regions (IC:SC, $P < 0.001$; IC:VC, $P < 0.001$; n = 7 animals, one-way ANOVA with Tukey post hoc) (Figure 4G). As epifluorescence imaging can be affected by photon scatter through brain tissue, our measurements likely overestimate the degree of correlation between IC and SC due to the proximity of these structures.

To assess whether tonotopic information is preserved as activity propagates from IC, through the thalamus to AC, we examined the spatial distribution of active neurons in AC during each spontaneous event detected in IC. Regions of interest (ROIs) were placed across the tonotopic axis of IC (Figure 4H,I) and regions of AC that exhibited correlated activity were assigned a color, corresponding to the region of IC (ROI) where correlated activity occurred (Figure 4J). Neurons within the central region of IC (blue color, Figure 4H) that later become responsive to low sound frequencies, exhibited correlated activity with neurons confined to three distinct areas of AC (Figure 4J-L and Movie S4), while events that occurred in lateral parts of the IC, corresponding to higher frequency regions (red color, Figure 4H), exhibited correlated activity within AC that surrounded these three areas (Figure 4J). Summing events over ten minutes allowed us to generate a color map relating AC neuron activity to IC isofrequency zones (Figure 4K-M). Previous studies indicate that low frequency sounds elicit neuronal activity in three distinct areas of AC (AI, AII, and AAF) (Issa et al., 2014; Stiebler et al., 1997), a pattern similar to the three AC regions that were correlated with low frequency regions of IC (blue color map, Figure 4K,L). Because epifluorescence imaging only allows optical access to the most dorsal aspect of IC (corresponding to frequencies up to ~16–24kHz), regions of AC that will be responsible for processing ultrasonic frequencies are less defined in the map (Figure 4L,M). Together, these

results indicate that local activity generated in the cochlea propagates through different auditory centers of the brain within spatially restricted zones that correspond to future isofrequency regions responsible for processing similar frequencies of sound.

Although the consistent delay in events between AC and IC suggests that activity propagates from the periphery to the cortex, it does not preclude cortical modulation of midbrain activity, which prominently influences activity patterns in IC in hearing animals (Yan and Ehret, 2002). To assess whether spontaneous activity in the IC is shaped by top-down projections, the AC was resected prior to imaging the midbrain (Figure S5A,B). Remarkably, spontaneous events persisted in both lobes of the IC following unilateral ablation of the AC (Figure S5A). Moreover, the frequency, amplitude, and half-widths of spontaneous events and the spatial distribution of events across each IC (Figure S5C,D) were unaltered by this manipulation, suggesting that reciprocal interactions between AC and IC are not functional at this stage of development.

Spontaneous activity in auditory centers persists in deaf mice

Sound energy is transformed into patterns of neural activity in the cochlea at glutamatergic synapses between IHCs and spiral ganglion neurons (SGNs) (Bobbin, 1979; Seal et al., 2008). These synapses are also required for propagating spontaneous activity prior to hearing onset, as correlated bursts of activity in SGNs are abolished *in vitro* in the presence of glutamate receptor antagonists (Tritsch et al., 2007; Zhang-Hooks et al., 2016). To examine whether glutamatergic synaptic transmission in the cochlea is required for IC activity *in vivo,* we applied Gelfoam containing the AMPA receptor antagonist NBQX to the semi-permeable round window membrane, an approach that has been used previously to deliver drugs to the inner ear without disrupting the organ of Corti (Harada et al., 1986). Unilateral exposure to NBQX mimicked the effect of unilateral cochlear ablation (Figure 3F), producing a significant reduction in the amplitude of spontaneous events in the contralateral IC (Figure 5A), indicating that spontaneous activity in central auditory centers relies on intact glutamatergic signaling between IHCs and SGNs in the cochlea.

Glutamatergic transmission between IHCs and SGNs is critically dependent on the vesicular glutamate transporter VGLUT3. Vesicular glutamate release at IHC-SGN synapses is abolished in *Vglut3*$^{-/-}$ (knockout, KO) mice and *Vglut3* KO mice are profoundly deaf at hearing onset (Seal et al., 2008; Figure S3F). Moreover, mutations in *Vglut3* lead to progressive loss of high frequency hearing in humans (Ruel et al., 2008). Although *Vglut3* KO mice exhibit aberrant refinement of connections in the auditory brainstem (Noh et al., 2010), it is not known how early patterns of activity in the CNS are influenced by loss of this critical peripheral input. To determine how genetic disruption of IHC-SGN synaptic transmission influences activity patterns in central auditory centers prior to hearing onset, we recorded spontaneous activity in *Snap25-T2A-GCaMP6s;Vglut3*$^{-/-}$ mice. Given the reduction of activity seen in the auditory midbrain following peripheral NBQX application and the complete block of SGN firing by AMPA receptor/NMDA receptor antagonists in acutely isolated cochleae (Tritsch et al., 2007; Zhang-Hooks et al., 2016), we predicted that spontaneous activity in the brain would be abolished in *Vglut3* KO mice. Unexpectedly, *Vglut3* KO mice displayed robust calcium increases in the IC that were remarkably similar

to activity observed in control mice (Figure 5B; Movie S5): Events were transient, bilateral, spatially restricted within each lobe of the IC and oriented along the tonotopic axis (Figure 5C). Nevertheless, normal activity patterns were not entirely preserved, as spontaneous events in *Vglut3* KO mice were less frequent, shorter in duration and larger in amplitude than events in control mice (Figure 5D, E, F). As expected, application of NBQX to the round window niche in *Vglut3* KO mice failed to lateralize activity (Figure 5G), indicating that burst firing of SGNs is induced without AMPA receptor-dependent excitation. Nevertheless, spontaneous activity in *Vglut3* KO mice remained dependent on input from the cochlea, as bilateral cochlear removal resulted in a marked reduction in IC activity (Figure S6).

Enhanced excitability of SGNs in *Vglut3* KO mice enables direct excitation by supporting cells

Previous studies indicate that SGN burst firing is induced by the periodic depolarization of IHCs in response to ATP-induced potassium release from nearby supporting cells (Wang et al., 2015). Due to the proximity of SGN dendrites to inner supporting cells, these local increases in potassium also depolarize afferent terminals, as shown through direct recordings from SGN dendrites (Tritsch et al., 2007); however, these depolarizations are not sufficient to induce SGN firing in control mice without IHC synaptic input. Attenuation of synaptic excitation in developing neurons has been shown to induce marked increases in intrinsic excitability (Shepherd et al., 2006; Turrigiano et al., 1998). When deprived of glutamatergic input, SGNs may similarly enhance their sensitivity to focal increases in potassium to enable action potential generation. Such a mechanism would explain the preservation of tonotopic spontaneous activity patterns in *Vglut3* KO mice; however, a similar outcome could be achieved if ATP-induced stimulation of supporting cells was indirectly enhanced by this manipulation of IHCs.

To determine if ATP-induced activity in supporting cells is enhanced in *Vglut3* KO mice, we recorded both spontaneous ATP-induced crenations in Kölliker's organ (Tritsch et al., 2007), which reflect the efflux of water that accompanies chloride and potassium efflux, and ATP-induced currents in inner supporting cells in cochleae acutely isolated from *Vglut3* KO mice. If ATP release is enhanced, spontaneous crenations should be larger in area and spontaneous inward currents should be larger in amplitude. However, ATP-induced crenations occurred at the same frequency and had the same average area in *Vglut3* KO mice as controls (Figure 6A,B). Moreover, the frequency and amplitude of spontaneous currents in supporting cells were comparable between control and *Vglut3* KO mice (Figure 6C,D), suggesting that ATP release is not enhanced. As the spontaneous currents in supporting cells arise from chloride efflux through TMEM16A calcium-activated channels (Wang and Bergles, 2014), and the release of potassium from supporting cells is directly coupled to this chloride efflux, the lack of increase in these currents also suggests that potassium release is not enhanced in *Vglut3* KO mice.

Although SGNs no longer receive synaptic excitation in *Vglut3* KO mice, the preservation of cochlea-dependent activity in central auditory centers suggests that these peripheral neurons continue to experience periodic excitation during this early period of development.

To define the activity patterns of SGNs in *Vglut3* KO mice, we performed timelapse confocal imaging of the spiral ganglion in cochleae isolated from *Snap25-T2A-GCaMP6s* mice. In control mice *(Vglut3+/+* littermates), groups of neighboring SGNs within the ganglion exhibited highly correlated, transient increases in calcium (Figure 6E; Movie S6). This activity was abolished by NBQX (50 μM; Figure 6E,F), consistent with prior results demonstrating that synaptic input is essential to trigger burst firing of SGNs at this age (Tritsch et al., 2007; Zhang-Hooks et al., 2016). Remarkably, SGNs in *Vglut3* KO mice also exhibited transient increases in calcium that were coincident among neighboring neurons (Figure 6G; Movie S7). Overall, these events were less frequent without IHC input (Figure 6F,H), fewer cells participated in each event (Figure 6I) and the degree of correlation was slightly reduced (Figure 6J). However, SGNs in *Vglut3* KO mice often exhibited prolonged plateau-like increases in calcium (Figure 6G,K,L, red asterisks), a behavior rarely observed in controls (Figure 6E, K), suggesting that they experience bouts of prolonged firing. As expected, spontaneous SGN activity in *Vglut3* KO mice was no longer blocked by NBQX (50 μM), indicating that these events are not induced by glutamatergic synaptic excitation (Figure 6G,H). To assess whether periodic activation of SGNs in *Vglut3* KO mice remains dependent on potassium release from supporting cells, we inhibited TMEM16A channels with benzbromorone (BBE, 20 μM) (Huang et al., 2012; Wang et al., 2015). This manipulation abolished SGN activity in *Vglut3* KO mice (Figure 6G,H), indicating that TMEM16A-facilitated release of potassium from supporting cells directly induces SGN burst firing.

To determine how SGNs are able to preserve burst firing in the absence of synaptic input, we measured the excitability of these neurons in whole-cell current-clamp recordings from acutely isolated cochleae (Figure 7A). In response to suprathreshold depolarizing current injection, SGNs in control mice *(Vglut3+/- or +/+* littermates) fired a single action potential at the onset of stimulation (11/12 cells; Figure 7B), as previously described (Rutherford et al., 2012), and exhibited a shallow current-to-voltage curve, due to their moderate membrane resistance (Figure 7C, G). In marked contrast, SGNs in *Vglut3* KO mice typically fired multiple action potentials in response to depolarizing current injection (13/19 cells; Figure 7C), and exhibited a much steeper current-to-voltage curve (Figure 7D) and longer membrane time constant (Figure 7F, G), due to their higher membrane resistance. Although control and *Vglut3* KO SGNs exhibited similar resting membrane potentials (Figure 7G), much less current was required to elicit action potentials in *Vglut3* KO SGNs (Figure 7B, D, G), providing an explanation for their enhanced sensitivity to changes in extracellular potassium. Moreover, some SGNs in *Vglut3* KO mice (6/19 cells) exhibited plateau potentials in response to depolarizing current steps, and similar long duration events occurred spontaneously in the absence of current injection (Figure 7H), in accordance with the long-duration calcium transients observed during time-lapse imaging (see Figure 6G). Together, these results indicate that SGNs exhibit much higher excitability when deprived of synaptic input from IHCs, which enables direct excitation by supporting cell-induced potassium transients.

DISCUSSION

Sensory systems exhibit robust, sensory-independent or "spontaneous" activity during a critical developmental period when neuronal specification, physiological maturation and synaptic refinement are ongoing. In the mouse auditory system, this period begins shortly after birth and continues until hearing onset almost two weeks later, providing an opportunity to explore the features of this activity and the mechanisms responsible *ex-utero.* Electrophysiological recordings have revealed that neurons in the auditory system fire periodic bursts of action potentials prior to hearing onset, a phenomenon that is conserved from birds to humans (Wang and Bergles, 2014). However, the spatial and temporal characteristics of this activity in relation to future tonotopic zones, the modification of activity patterns as they ascend through different auditory centers and the relationship of this peripherally generated activity to other forms of spontaneous activity in the brain have not been defined.

Insight into the relationship between spontaneous activity and circuit development have been difficult to obtain using electrophysiological approaches, due to their limited spatial sampling and the need to record under anesthesia to limit mouse movement, which may induce unknown alterations in neuronal firing in these nascent circuits. To overcome these limitations, we performed *in vivo* imaging of neuronal calcium changes in central auditory centers of awake, unanesthetized mice before hearing begins, allowing visualization of internally generated neuronal activity patterns across wide spatial and temporal scales. Our studies indicate that groups of neurons aligned to future isofrequency zones in the auditory midbrain exhibit highly correlated, transient bursts of activity. This activity is initiated within the cochlea and propagates through auditory centers before ultimately reaching the auditory cortex, indicating that the activity of neurons responsible for processing similar frequencies of sound are coordinated across the entire auditory system during this phase of development. Our results also reveal that developing auditory circuits exhibit remarkable homeostatic plasticity that enables this early patterned activity to be preserved despite disruption of synaptic communication between IHCs and SGNs. The ability of SGNs to adapt to genetic disruption of sensory transduction during this critical developmental period may help preserve auditory nerve fibers and promote early maturation of tonotopic pathways, enabling individuals who carry mutations in these key components to achieve greater benefit from cochlear implants or genetic therapies designed to correct these mutations.

Tonotopic neural activity in developing auditory centers

Macroscopic imaging of the dorsal aspect of the IC in transgenic mice that express GCaMP6s under control of the *Snap25* promoter (Madisen et al., 2015), a v-snare expressed ubiquitously by both excitatory and inhibitory neurons, revealed that neurons in this midbrain auditory center exhibit highly stereotyped patterns of activity before hearing onset. Both postsynaptic target neurons, and the ascending afferents responsible for inducing their excitation, experience transient increases in calcium lasting several seconds. Such long duration events are consistent with electrophysiological recordings from prehearing rats indicating that neurons within the auditory brainstem and midbrain fire discrete bursts of

action potentials followed by long periods of quiescence (Clause et al., 2014; Crins et al., 2011; Sonntag et al., 2009; Tritsch et al., 2010b). Two photon imaging revealed that IC neurons are excited on average 2–3 times per minute by these events (Figure 2), closely following the pattern of activity exhibited by auditory neurons in the spiral ganglion, medial nucleus of the trapezoid body, and cochlear nucleus (Clause et al., 2014; Sonntag et al., 2009; Tritsch et al., 2010b), showing that this mode of generating infrequent, but intense, bouts of neuronal activity is preserved as signals progress through higher auditory centers. The clustering of action potentials into discrete bursts may ensure that activity reliably propagates through these developing circuits, overcoming stochastic variation and nascent synapses with low release probability (Gasparini et al., 2000), and inducing long-lasting calcium rises capable of initiating changes in gene expression that underlie structural and functional maturation.

Both wide field epifluorescence and high resolution two photon imaging revealed that spontaneous events in the IC involved clusters of neurons aligned to the future tonotopic axis. Neurons in the IC assemble into fibrodendritic laminae that are highly conserved across species and comprised of afferent lemniscal fibers and dendrites of intrinsic neurons, which provide a structural basis for the restricted activation of neurons within discrete isofrequency zones (Malmierca et al., 1995). Similar laminar, tonotopic projections are prevalent in other subcortical auditory centers (Kandler et al. 2009), enabling events that are initiated through excitation of a group of IHCs within one region of the cochlea to remain confined to this frequency domain as it ascends through the auditory system. Although individual events were spatially restricted to a portion of the IC, events occurred throughout all regions of the IC that could be imaged using the approaches employed here. Thus, these events fulfill key tenants of Hebbian rules for plasticity, triggering correlated firing of ascending afferents and postsynaptic target neurons that will eventually process similar frequencies of sound, providing a means for activity-dependent refinement and stabilization of synaptic connections within distinct frequency domains.

Mechanisms responsible for spontaneous activity prior to hearing onset

Although the IC in adult animals has been shown to integrate multisensory information, it is striking how restricted active input to the IC is prior to hearing onset. Bilateral ablation of the cochlea nearly abolished all bursting activity in the IC. Exceptions were infrequent, large scale events that engaged neurons throughout these midbrain structures (0.8 ± 0.1 events per minute, n = 8 animals; Figure S7). The mechanisms that coordinate activity across different sensory processing circuits remain unknown, but could be induced by neuromodulatory inputs such as cholinergic fibers, which are highly ramified within the midbrain (Klepper and Herbert, 1991). Despite functional evidence for powerful top-down cortical modulation of the IC in hearing animals (Yan and Ehret, 2002), our studies also indicate that there is limited modulation of IC activity by descending projections from AC at this developmental stage, as unilateral ablation of the AC did not alter activity patterns in the ipsilateral IC (Figure S5). From the standpoint of circuit integration, it may be advantageous to delay establishment of pathways responsible for feedback control and cross-modal integration until direct sensory processing pathways are stabilized. It is also possible that the

stereotyped firing pattern exhibited by neurons at this developmental stage lacks components necessary to effectively engage these pathways.

Bilateral ablation of the cochlea abolished coincident, spatially restricted neuronal activity in the IC (Figure 3), indicating that it is dependent on input from these developing sensory organs. Our previous studies indicate that IHCs along the organ of Corti are transiently excited when inner supporting cells release ATP, triggering a cascade of events in these cells that ultimately results in release of potassium that induces IHC depolarization (Tritsch et al., 2007; Wang et al., 2015). These ATP-triggered events are spatially restricted, resulting in depolarization of IHCs within discrete regions along the cochlea; they are distributed, encompassing all frequency domains along the length of the cochlea; they are stochastic, appearing in random positions along organ of Corti; and they are highly variable in amplitude and duration, triggering activation of different numbers of IHCs during each event (Tritsch and Bergles, 2010; Wang et al., 2015). These defining features are also shared by events in the IC at this age, providing additional *in vivo* support for the hypothesis that this mechanism is primarily responsible for driving the correlated firing of auditory neurons during this stage of development. It is possible that other mechanisms contribute to excitation of IHCs prior to hearing onset, particularly at younger ages before TMEM16A channels are expressed (Johnson et al., 2011, 2012; Wang et al., 2015), similar to the transition in mechanisms responsible for inducing retinal waves prior to eye opening (Kirkby et al., 2013). Indeed, recent *in vivo* recordings from neurons in the medial nucleus of the trapezoid body of pre-hearing mice in which efferent cholinergic modulation of IHCs was abolished, revealed that modulatory projections from the brainstem to the cochlea influence the timing and duration of bursts at this age (Clause et al., 2014).

Preservation of spontaneous activity in absence of hair cell synaptic transmission

Propagation of spontaneous activity from the cochlea to the CNS in wild type animals is critically dependent on synaptic excitation of SGNs, as acute pharmacological block of ionotropic glutamate (AMPA/NMDA) receptors abolishes correlated firing of SGNs in isolated cochleae (Figure 6; Zhang-Hooks et al., 2016), and local application of the AMPA receptor antagonist NBQX to the round window membrane *in vivo* biased event amplitudes in the IC to the ipsilateral side, mimicking the effect of unilateral cochlea ablation (Figure 3). These findings are consistent with results from paired IHC-SGN recordings, which indicate that bursts of action potentials are initiated in SGNs only when IHCs fire calcium action potentials (Tritsch et al., 2010b). However, SGN dendrites are located in regions of Kölliker's organ where ATP is released (see Figure 6A), and direct recordings from SGN dendritic boutons revealed that they are depolarized by ATP-induced potassium release from inner supporting cells (Tritsch et al., 2007), although the magnitude of these events is not sufficient to trigger burst firing without synaptic input. These findings suggest that manipulations that disrupt calcium-dependent glutamate release from IHCs should abolish spontaneous activity in central auditory centers. However, our studies indicate that spontaneous activity still occurs in the IC in *Vglut3* KO mice, in which synaptic excitation of SGNs in abolished (Seal et al., 2008). Perhaps more surprising, the pattern of activity in these mice shares many key features of spontaneous activity in wild type animals, in particular the restriction of events to isofrequency zones, suggesting that they arise through

activation of SGNs that receive input from restricted regions along the organ of Corti. Previous studies have shown that CNS neurons undergo homeostatic increases in excitability when deprived of synaptic excitation (Turrigiano et al., 1998). These changes can involve an increase in number of AMPA receptors at synapses to enhance synaptic potency and a decrease in potassium channel expression to enhance depolarization to each input (Lee et al., 2015; Shepherd et al., 2006). Whole cell recordings revealed that SGNs in *Vglut3* KO mice have higher input resistance, a longer membrane time constant and a lower current threshold for action potential initiation, allowing normally subthreshold responses to restore firing without input from IHCs. Moreover, some neurons exhibited unusual plateau-like potentials upon depolarization that outlasted the stimulus, which may contribute to long duration calcium transients seen with GCaMP imaging. Our studies also reveal that there are further downstream changes in central auditory circuits in *Vglut3* KO mice, as noted previously (Noh et al., 2010), which allow occasional, tonotopic bursts to be generated after bilateral cochlea ablation (Figure S6). Although the mechanisms responsible for these changes remain to be determined, recent studies indicate that maturation of SGNs is delayed in *Vglut3* KO mice (Sun et al., in press) pointing to an important role for synaptic activity in shaping the excitability of these neurons prior to hearing onset.

The ability of peripheral ganglion neurons to change their excitability through alteration of intrinsic ion channel expression has been observed in dorsal root ganglion following traumatic injury (Dib-hajj et al., 1999; Song et al., 2003). However, to our knowledge, this is the first demonstration that spiral ganglion neurons exhibit enhanced excitability when deprived on synaptic excitation. If SGNs retain this ability to adjust their excitability after hearing onset, these changes could contribute to hyperactivity in the auditory pathway following damage- or age-induced loss of IHCs (Salvi et al., 2000). Activity also plays a crucial role in promoting neuronal survival in the developing CNS (Spitzer, 2006). The ability of SGNs to preserve burst firing in the absence of excitatory drive from IHCs may help explain why most SGNs do not undergo apoptosis in *Vglut3* KO mice (Seal et al., 2008). Further studies of activity patterns in *Vglut3* KO mice, and animals that harbor deafness-inducing mutations in other genes, will help define the extent of both early and persistent changes in auditory circuits. This analysis may reveal new strategies for enhancing hearing in deaf individuals and promoting functional recovery after traumatic injury to the cochlea.

STAR METHODS

CONTACT FOR REAGENT AND RESOURCE SHARING

Further information and requests for resources and reagents should be directed to and will be fulfilled by the Lead Contact, Dwight Bergles (dbergles@jhmi.edu).

EXPERIMENTAL MODEL AND SUBJECT DETAILS

Both male and female mice of postnatal days (P) 6 - P15 were used for all experiments and randomly allocated to experimental groups. All mice were healthy and were only used for experiments detailed in this study. Transgenic breeders were crossed to female FVB mice to improve litter survival and, thus, progeny were not maintained on a pure C57BL/6

background. Mice were housed on a 12 hour light/dark cycle and were provided food ad libitum. All experiments and procedures were approved by the Johns Hopkins Institutional Care and Use Committee.

Transgenic Animal Models

Snap25-T2A-GCaMP6s and *VGLUT3⁻/⁻ (Vglut3* KO) have been described previously (Madisen et al., 2016; Seal et al., 2008).

Method Details

Installation of cranial windows—Inhalation anesthesia was induced with vaporized isoflurane (4% for 5 minutes, or until mice are non-responsive to toe-pinch) and lowered during the procedure (1–2%) to maintain a stable respiration rate of 80 breaths per minute. A midline incision beginning posterior to the ears and ending just anterior to the eyes was made. Two subsequent cuts were made to remove the dorsal surface of the scalp. A headbar was secured to the head using super glue (Krazy Glue). Fascia and neck muscles overlying the interparietal bone were resected and the area bathed in sterile, HEPES-buffered artificial cerebrospinal fluid that was replaced as necessary throughout the surgery. Using a 28G needle and microblade, the sutures circumscribing the interparietal bone were cut and the interparietal bone was removed to expose the midbrain. The dura mater was removed using fine scissors and forceps, exposing the colliculi and extensive vasculature. If the animal was to be imaged under the two-photon microscope, astrocytes were labeled by applying 1 μM sulfarhodamine 101 (SR101) in HEPES-ACSF for five minutes to the surface of the brain. A 5 mm coverslip (CS-5R; Warner Instruments) was then placed over the craniotomy, the surrounding bone was dried using a Kimwipe, and super glue was placed along the outer edges of the coverslip for adhesion to the skull. Replacement 0.9% NaCl solution was injected IP and a local injection of lidocaine was given to the back of the neck. Animals were weaned off isoflurane, placed under a warming lamp, and allowed to recover for a minimum of 1 hour prior to imaging. As reported previously (Ackman et al., 2012), spontaneous activity was not seen in deeply anesthetized animals and emerged ~30 minutes after recovery from isoflurane exposure.

For simultaneous imaging of IC and AC, mice were anesthetized as described above. The scalp was resected and a head-bar affixed to the skull with superglue. A cranial window over the auditory cortex (AC, ~3.5 mm lateral to lambda) was made using a micro-blade to shave away the bone overlying a region encompassing AC starting from the lateral suture and moving medially (~3 to 4 mm diameter). The AC window area was covered with HEPES-ACSF throughout the procedure. The dura was carefully removed before a glass cover slip (CS-4R; Warner Instruments) was glued over the window. IC cranial windows were made and animals recovered as described above.

Delivery of agents to the round window niche—Prior to cranial window installation, a postauricular incision was made and the cervical musculature retracted to expose the auditory bulla. Using microscissors, the posterior region of the bulla, just ventral to the facial nerve, was removed and the middle ear exposed. To visualize the round window niche and window, extraneous mesenchyme was removed using dental absorbent paper points.

Gelfoam soaked in specific pharmacological agents (made up in isotonic, 5% mannitol solution; NBQX 50 mM) was placed within the round window niche against the semi-permeable round window membrane. After Gelfoam placement, the overlying muscles were moved back into place and the incision was closed with Vetbond. Animals were imaged within 1.5 hours after drug application.

Auditory cortex ablation—Prior to cranial window installation, an incision in the skull was made just posterior to the right auditory cortex. Auditory cortex tissue was then aspirated via a glass pipette tip coupled to a suction line. Gelfoam was packed into the volume removed and the wound closed with super glue (Vetbond). Following imaging, animals were perfused with 4% PFA and brains harvested. Brains were embedded in 2% agarose and sectioned for post-hoc analysis of cortex removal.

***In vivo* calcium imaging—**After 1 hour of post-surgical recovery from anesthesia, pups were moved into a swaddling 15 mL conical centrifuge tube. The top half of this tube was removed to allow access to the headbar and visualization of the craniotomy. Pups were head-fixed and maintained at 37°C using a heating pad and temperature controller (TC-1000; CWE). During the experiments, pups were generally immobile; however, occasional limb and tail twitching did occur.

For wide field epifluorescence imaging, images were captured at 10 Hz using a Hamamatsu ORCA-Flash4.0 LT digital CMOS camera coupled to a Zeiss Axio Zoom.V16 stereo zoom microscope. For midbrain imaging, a 4×4 mm field of view was illuminated continuously with a mercury lamp (Zeiss Illuminator HXP 200C) and visualized through a 1X PlanNeoFluar Z 1.0× objective at 17× zoom. For simultaneous imaging of cortex and midbrain, a 6×6 mm field of view was imaged at 11× zoom. Images were captured at a resolution of 512×512 pixels (16-bit pixel depth) after 2×2 binning to increase sensitivity. Each recording consisted of uninterrupted acquisition over 10 minutes.

A two-photon microscope (Bergamo II; Thorlabs) was used to capture high resolution images of spontaneous activity in the dorsal aspect of the central nucleus of the inferior colliculus (IC). Two photon excitation was achieved using a Ti:sapphire laser (Chameleon Ultra II; Coherent) tuned to 920 nm. A 533×533 μm field of view was visualized using a 25× Nikon objective (N25X-APO-MP). Images were collected at a resolution of 512×512 pixels (16-bit pixel depth) at 30 Hz using a galvo-resonant scanner and subsequently averaged to produce a final framerate of 10 Hz. Each recording consisted of uninterrupted acquisition over 10 minutes.

Image processing—For wide field imaging, raw images were imported into the ImageJ environment and corrected for photobleaching by fitting a single exponential to the fluorescence decay and subtracting this component from the signal (Bleach Correct function, exponential fit). Images were then imported into MATLAB (Mathworks) and intensities were normalized as $\Delta F/F_o$ values, where $\Delta F = F - F_o$ and F_o was defined as the fifth percentile value for each pixel. Ovoid regions of interest (ROIs) encompassing the entire left and right inferior colliculi were drawn (see Figure 1D). Across all conditions, the size of the ROIs was invariant, however, due to small differences in the imaging field between animals,

the ROIs were placed manually for each imaging session. Peaks in the signals were detected in MATLAB using the built-in peak detection function (findpeaks) using a fixed value threshold criterion; because fluorescence values were normalized, this threshold was fixed across conditions (2% F/F_O). Occasionally, large events in the cortex or superior colliculus would result in detectable fluorescence increases in the IC. These events broadly activated the entire surface of the IC and did not exhibit the same spatially-confined characteristics as events driven by the periphery. These events were not included in the analysis (see Figure S7).

For two-photon imaging, images were imported into ImageJ for registration. The red channel (SR101) was registered (MultiStackReg; translation) and the transformation matrices applied to the green channel (GCaMP6s). Registered images were imported into MATLAB and intensities were normalized as F/F_O values as described above. For analysis of neurons and neuropil, ten random x-y locations were generated in MATLAB and ROIs manually drawn around the nearest neuron and surrounding neuropil. Peaks in signals were detected in MATLAB using the built-in peak detection function (findpeaks) using a fixed value threshold criterion (mean + 3 standard deviations for each cell).

For determining periods of animal movement during simultaneous imaging of AC and IC, a small section of the image with prominent movement artifacts was used as the basis for movement detection. This image was subject to image registration (dftregistration function, Matlab; Guizar-sicairos et al., 2008) and the transformation matrices used to align the images were stored. We then took the magnitude (norm) of the transformation matrix to determine periods of movement. When the image is stable, the magnitude of the transformation matrix equates to 1. When the image shifts, the magnitude of the transformation matrix exceeds 1. Periods of movement were defined as extended periods (> 3 frames) where the magnitude of the transformation matrix was greater than 1.

Generation of spatial correlation maps—For generation of spatial correlation maps within and across IC (as seen in Figure 2E, 4H, and S2E), ROIs (10×10 pixels) were placed across the tonotopic axis as indicated. These signals served as spatial correlation seeds and were used to generate spatial correlation maps. This was done by computing the correlation value between the seed signal and every pixel in the image. Each seed generated a single map which was then placed into a distinct color channel. The aggregate of all spatial correlation maps, each within its own color channel, results in the panels shown. Because of prominent photon scattering and background fluorescence, correlation maps appear more diffuse and contain more gray values calculated using epifluorescence images (Figure 4H and S2E) than in correlation maps produced using two-photon excitation (Figure 2E).

For generation of spatial correlation maps between IC and auditory cortex (as seen in Figure 4B), an ROI was manually drawn around the IC and correlations were calculated for each pixel across the entire image. Pixels with an r value greater than 0.8 were defined as auditory cortex. A similar approach was used to delineate boundaries of the visual cortex with signals in the superior colliculus. Pearson's correlation coefficients were calculating using the normalized fluorescence intensity.

Generation of auditory cortex maps—ROIs were placed across the future tonotopic axis of the IC and fluorescent signals normalized as described above and mean subtracted. For each IC ROI, peaks of minimum height 3% $\Delta F/F_o$ were detected and the channel with the greatest $\Delta F/F_o$ was used to determine the location of the peak. AC activity corresponding to those peaks was averaged (weighted by IC peak height). The AC map for each animal was generated by taking each average AC image (corresponding to activity at different tonotopic areas in the IC), and placing them into a distinct color channel (blue representing the most medial single bands, future low frequency zones, and red representing the most lateral bands, future higher frequency zones). Responding areas were delimited by thresholding the average image at 80% maximum response. The average tonotopic map across animals was generated by a threshold of 50% across the smoothed average image of thresholded maps.

Auditory stimulation—Sounds were presented using a free-field speaker (MF1; Tucker-Davis Technologies) placed 10 cm from the left ear. For wide field imaging, animals were placed in a custom-made sound isolation chamber that attenuated outside noises by 40 dB SPL. Calibration of noise levels was performed using an ultrasonic probe (Sokolich). Stimuli consisted of sinusoidal amplitude modulated tones (1 s, 10 Hz modulation) from 3kHz to 96kHz. All stimuli were cosine-squared gated (5 ms) and played in a random order at 5 second intervals. Intensity levels were not flat across the entire range of the speaker (Figure S3) and no level correction was applied. Because thresholds are very high in animals just after hearing onset, all tones were presented at 0 dB attenuation. Tones were generated within the RPvdsEx software, triggered using the microscope's frame out signal, and delivered through the RZ6 Audio Processor (Tucker-Davis technologies). During imaging, vocalizations and ambient noise were captured using the Sokolich ultrasonic probe and digitized at 196kHz through the RZ6 Audio Processor.

Electrophysiology—For inner supporting cell recordings, apical segments of the cochlea were acutely removed from P6-P8 control or *Vglut3* KO mice and used within 2 hours of the dissection. For spiral ganglion neuron recordings, middle segments of the cochlea were acutely removed from P5-P7 control or *Vglut3* KO mice and used immediately, or were placed into culture media (DMEM as described below) and used within 4 hours. Cochleae were then moved into a recording chamber and continuously superfused with bicarbonate-buffered artificial cerebrospinal fluid (1.5 – 2 mL/min) consisting of the following (in mM): 115 NaCl, 6 KCl, 1.3 $MgCl_2$, 1.3 $CaCl_2$, 1 NaH_2PO_4, 26.2 $NaHCO_3$, 11 D-glucose, and saturated with 95% O_2 / 5% CO_2 to maintain a pH of 7.4. Solutions were superfused at near physiological temperature (32–34°C) using a feedback-controlled in-line heater (Warner Instruments) for all experiments except those indicated as 24°C in Figure 7. Whole-cell recordings of inner supporting cells (ISCs) and spiral ganglion neurons (SGNs) were made under visual control using differential interference contrast microscopy (DIC). Electrodes had tip resistances between 3.5–4.5 MΩ when filled with internal consisting of (in mM): 134 KCH_3SO_3, 20 HEPES, 10 EGTA, 1 $MgCl_2$, 0.2 Na-GTP, pH 7.3. Spontaneous currents were recorded with ISCs held at –80mV. Errors due to the voltage drop across the series resistance and the liquid junction potential were left uncompensated. Recordings that displayed more than 10% increase in access resistance were discarded. Spontaneous currents were recorded with pClamp 10 software using a Multiclamp 700B amplifier, low pass

filtered at 2 kHz, and digitized at 5 kHz with a Digidata 1322A analog-to-digital converter (Axon Instruments). Voltage responses to current injections in SGNs were recorded were low pass filtered at 20 kHz, and digitized at 50 kHz.

Analysis of intrinsic membrane properties—Series of current steps were injected into SGNs with start and end points not exceeding −100 mV and −20 mV steady state membrane potentials. Input resistances were calculated by taking the peak (min or max of signal through first 20% of current step) or the steady state voltage change (last 100 ms of step). Tau was calculated by fitting a single exponential curve between 10 and 90% maximum voltage change to a −2.5 pA current injection. Current threshold for action potential generation was measured by increasing steps in 5 pA increments until an action potential occurred.

Transmitted light imaging—Cochlear segments were imaged with a 40× water immersion objective and recorded using MATLAB and a USB capture card (EZ Cap). Difference movies were generated by subtracting frames at time t_n and t_{n+5} seconds using ImageJ software to generate an index of transmittance change over time. To quantify transmittance changes, a threshold of three standard deviations above the mean was applied to the values. To calculate the frequency of these events, the whole field was taken as an ROI and peaks were detected using MATLAB (findpeaks function). To calculate area of these events, a Gaussian filter (sigma = 2.0) was applied to the image after thresholding and the borders detected using MATLAB (bwlabel function). The area was then calculated as the number of pixels within the border multiplied by the area scaling factor $(\mu m/pixel)^2$.

Cochlear explant culture—Cochleae were dissected from P5 control *(Snap25-T2A-GCaMP6s)* and *Vglut3* KO mice *(Snap25-T2A-GCaMP6s; VGLUT3T$^{-/-}$)*, as described previously (Tritsch et al., 2007; Zhang-Hooks et al., 2016). The cochleae were acutely dissected in ice-cold, sterile-filtered HEPES-buffered ACSF consisting of the following (in mM): 130 NaCl, 2.5 KCl, 10 HEPES, 1 NaH$_2$PO$_4$, 1.3 MgCl$_2$, 2.5 CaCl$_2$, and 11 D-Glucose. Explants were mounted onto Cell-Tak (Corning) treated coverslips and incubated at 37°C for 24 hours in Dulbecco's modified Eagle's medium (F-12/DMEM; Invitrogen) supplemented with 1% fetal bovine serum (FBS) and 10U/mL penicillin (Sigma).

Confocal imaging of cochlear explants—After one day *in vitro*, cochleae were moved into a recording chamber and continuously superfused with bicarbonate-buffered artificial cerebrospinal fluid (1.5 – 2 mL/min) consisting of the following (in mM): 115 NaCl, 6 KCl, 1.3 MgCl$_2$, 1.3 CaCl$_2$, 1 NaH$_2$PO$_4$, 26.2 NaHCO$_3$, 11 D-glucose, and saturated with 95% O$_2$ / 5% CO$_2$ to maintain a pH of 7.4. Imaging was performed at near physiological temperature (32–34°C) using a feedback-controlled in-line heater (Warner Instruments). Images were captured at 1 frame per second using a Zeiss laser scanning confocal microscope (LSM 710, Zeiss) through a 20X objective (Plan APOCHROMAT 20×/1.0 NA) at 512 × 512 pixel (354 × 354 μm; 16-bit depth) resolution. Sections were illuminated with a 488nm laser (maximum 25mW power). NBQX (2,3-Dioxo-6-nitro-1,2,3,4-tetrahydrobenzo[*f*]quinoxaline-7-sulfonamide, 50 μM, Tocris) and benzbromarone (BBE, 20 μM, Sigma) were applied by addition to the superfusing ACSF. To elicit depolarization and

visualization of all ganglion neurons at the end of the experiment, explants were exposed to high potassium ACSF consisting of the following (in mM): 80 NaCl, 40 KCl, 1.3 MgCl$_2$, 1.3 CaCl$_2$, 1 NaH$_2$PO$_4$, 26.2 NaHCO$_3$, 11 D-glucose, and saturated with 95% O$_2$ / 5% CO$_2$ to maintain a pH of 7.4. Only cells which increased their fluorescence by 25% over baseline in response to high potassium were used for analysis.

Analysis of calcium transients in SGNs—Images were imported into ImageJ and image registration (MultiStackReg) was used to correct for slight drifts in the imaging field. Regions of interest were drawn around SGNs that exhibited increases in fluorescence in response to high potassium external solution. Fluorescence changes were normalized as F/F_o values, where $F = F - F_o$ and F_o was defined as the fifth percentile value for each pixel. Peaks in the signals were detected in MATLAB using the built-in peak detection function (findpeaks) with a fixed value threshold criterion (mean + 3 standard deviations for each cell). Across all cells, events were specified when three or more cells displayed peaks in fluorescence within a one second time window. For correlation analysis, the five nearest and farthest cells to a target cell were calculated using the center of mass of the ROI. Correlations on these groups of cells were calculated using normalized fluorescence signals.

Immunohistochemistry—Mice were deeply anesthetized with isoflurane and perfused with freshly prepared 4% paraformaldehyde in 0.1 M phosphate buffer. Brains were post-fixed for 45 minutes at room temperature and stored at 4°C until processing. Bra ins were embedded in 2% agarose gel and 50 μm sections were cut with a vibratome and mounted onto Superfrost Plus glass slides (Fisher). Sections were incubated overnight with primary antibodies against GFP (pChicken; 1:4000, Aves) and NeuN (pMouse; 1:500, Millipore). Sections were then rinsed three times with PBS and incubated for two hours at room temperature with secondary antibodies raised in donkey (Alexa-488 and Alexa-546; 1:2000, Life Technologies). Slides were washed three times in PBS, allowed to dry, and sealed using Aqua Polymount (Polysciences, Inc.). Images were captured using a laser scanning confocal microscope (LSM 710 Meta, Zeiss).

Quantification and statistical analyses

All statistics were performed in the MATLAB (Mathworks) programming environment. All statistical details, including the exact value of n, what n represents, and which statistical test was performed, can be found in the figure legends. Unless otherwise noted, data are presented as mean ± standard error of the mean. All datasets were tested for Gaussian normality using the D'Agostino's K^2 test. If datasets were normal, two-tailed paired t-tests were used. Otherwise, the nonparametric Mann-Whitney test was used. For single comparisons, significance was defined as $p <= 0.05$. When multiple comparisons were made, the Bonferroni correction was used to adjust p-values accordingly to lower the probability of type I errors. For multiple condition datasets, a one-way ANOVA or two-way ANOVA analysis was used, followed by Tukey's multiple comparison tests.

Supplementary Material

Refer to Web version on PubMed Central for supplementary material.

ACKNOWLEDGEMENTS

REFERENCES

Ackman JB, Burbridge TJ, and Crair MC (2012). Retinal waves coordinate patterned activity throughout the developing visual system. Nature 490, 219–225. [PubMed: 23060192]

Allen-Sharpley MR, and Cramer KS (2012). Coordinated Eph-ephrin signaling guides migration and axon targeting in the avian auditory system. Neural Dev. 7, 1–14. [PubMed: 22225949]

Barnstedt O, Keating P, Weissenberger Y, King AJ, and Dahmen JC (2015). Functional microarchitecture of the mouse dorsal inferior colliculus revealed through in vivo two-photon calcium imaging. J. Neurosci 35, 10927–10939. [PubMed: 26245957]

Bobbin RP (1979). Glutamate and aspartate mimic the afferent transmitter in the cochlea. Exp. Brain Res 34, 389–393. [PubMed: 217706]

Clause A, Kim G, Sonntag M, Weisz CJC, Vetter DE, Rubsamen R, and Kandler K (2014). The precise temporal pattern of prehearing spontaneous activity is necessary for tonotopic map refinement. Neuron 82, 822–835. [PubMed: 24853941]

Clause A, Lauer AM, Kandler K, and Morley BJ (2017). Mice lacking the alpha9 subunit of the nicotinic acetylcholine receptor exhibit deficits in frequency difference limens and sound localization. Front. Cell. Neurosci 11, 1–12. [PubMed: 28154525]

Coleman JR, and Clerici WJ (1987). Sources of projections to subdivisions of the inferior colliculus in the rat. J. Comp. Neurol 262, 215–226. [PubMed: 3624552]

Crins TTH, Rusu SI, Rodríguez-Contreras A, and Borst JGG (2011). Developmental changes in short-term plasticity at the rat calyx of held synapse. J. Neurosci 31, 11706–11717. [PubMed: 21832200]

Dib-hajj SD, Fjell J, Cummins TR, Zheng Z, and Fried K (1999). Plasticity of sodium channel expression in DRG neurons in the chronic constriction injury model of neuropathic pain. Pain 83, 591–600. [PubMed: 10568868]

Francis NA, Winkowski DE, Sheikhattar A, Armengol K, Babadi B, and Kanold PO (2018). Small networks encode decision-making in primary auditory cortex. Neuron 97, 885–897. [PubMed: 29398362]

Gasparini S, Saviane C, Voronin LL, and Cherubini E (2000). Silent synapses in the developing hippocampus : Lack of functional AMPA receptors or low probability of glutamate release? Proc. Natl. Acad. Sci 3–8.

González Hernández TH, Meyer G, and Ferres-Torres R (1986). The commissural interconnections of the inferior colliculus in the albino mouse. Brain Res. 368, 268–276. [PubMed: 2421840]

Guizar-sicairos M, Thurman ST, and Fienup JR (2008). Efficient subpixel image registration algorithms. Opt. Lett 33, 156–158. [PubMed: 18197224]

Harada T, Iwamori M, Nagai Y, and Nomura Y (1986). Ototoxicity of neomycin and its penetration through the round window membrane into the perilymph. Ann. Otol. Rhinol. Laryngol 404–408. [PubMed: 3740717]

Hind JE, Goldberg JM, Greenwood DD, and Rose JE (1963). Some discharge characteristics of single neurons in the inferior colliculus of the cat. II. Timing of the discharges and observations on binaural stimulation. J. Neurophysiol 26, 321–341. [PubMed: 13954634]

Huang F, Zhang H, Wu M, Yang H, Kudo M, Peters CJ, Woodruff PG, Solberg OD, Donne ML, Huang X, et al. (2012). Calcium-activated chloride channel TMEM16A modulates mucin secretion and airway smooth muscle contraction. Proc. Natl. Acad. Sci 109, 16354–16359. [PubMed: 22988107]

Issa JB, Haeffele BD, Agarwal A, Bergles DE, Young ED, and Yue DT (2014). Multiscale optical Ca2+ imaging of tonal organization in mouse auditory cortex. Neuron 83, 944–959. [PubMed: 25088366]

Johnson SL, Eckrich T, Kuhn S, Zampini V, Franz C, Ranatunga KM, Roberts TP, Masetto S, Knipper M, Kros CJ, et al. (2011). Position-dependent patterning of spontaneous action potentials in immature cochlear inner hair cells. Nat. Neurosci 14, 711–717. [PubMed: 21572434]

Johnson SL, Kennedy HJ, Holley MC, Fettiplace R, and Marcotti W (2012). The resting transducer current drives spontaneous activity in prehearing mammalian cochlear inner hair cells. J. Neurosci 32, 10479–10483. [PubMed: 22855797]

Johnson SL, Ceriani F, Houston O, Polishchuk R, Polishchuk E, Crispino G, Zorzi V, Mammano F, and Marcotti W (2017). Connexin-Mediated Signaling in Nonsensory Cells Is Crucial for the Development of Sensory Inner Hair Cells in the Mouse Cochlea. J. Neurosci 37, 258–268. [PubMed: 28077706]

Jones TA, Leake PA, Snyder RL, Stakhovskaya O, and Bonham B (2007). Spontaneous discharge patterns in cochlear spiral ganglion cells before the onset of hearing in cats. J. Neurophysiol 1898–1908. [PubMed: 17686914]

Kandler K, Clause A, and Noh J (2009). Tonotopic reorganization of developing auditory brainstem circuits. Nat. Neurosci 12, 711–717. [PubMed: 19471270]

Kilgard MP, and Merzenich MM (1998). Cortical map reorganization enabled by nucleus basalis activity. Science 279, 1714–1718. [PubMed: 9497289]

Kirkby LA, Sack GS, Firl A, and Feller MB (2013). A role for correlated spontaneous activity in the assembly of neural circuits. Neuron 80, 1129–1144. [PubMed: 24314725]

Klepper A, and Herbert H (1991). Distribution and origin of noradrenergic and serotonergic fibers in the cochlear nucleus and inferior colliculus of the rat. Brain Res. 557, 190–201. [PubMed: 1747753]

Lee KY, Royston SE, Vest MO, Ley DJ, Lee S, Bolton EC, and Chung HJ (2015). N-methyl-D-aspartate receptors mediate activity-dependent down-regulation of potassium channel genes during the expression of homeostatic intrinsic plasticity. Mol. Brain 8, 4. [PubMed: 25599691]

Lippe W (1994). Rhythmic spontaneous activity in the developing avian auditory system. J. Neurosci 14, 1486–1495. [PubMed: 8126550]

Madisen L, Garner AR, Shimaoka D, Chuong AS, Klapoetke NC, Li L, van der Bourg A, Niino Y, Egolf L, Monetti C, et al. (2015). Transgenic mice for intersectional targeting of neural sensors and effectors with high specificity and performance. Neuron 85, 942–958. [PubMed: 25741722]

Malmierca MS, Rees A, Le Beau FEN, and Bjaalie JG (1995). Laminar organization of frequency-defined local axons within and between the inferior colliculi of the guinea pig. J. Comp. Neurol 357, 124–144. [PubMed: 7673462]

Murata Y, and Colonnese MT (2016). An excitatory cortical feedback loop gates retinal wave transmission in rodent thalamus. Elife 5, 1–19.

Nimmerjahn A, and Helmchen F (2012). In vivo labeling of cortical astrocytes with sulforhodamine 101 (SR101). Cold Spring Harb. Protoc 7, 326–334.

Noh J, Seal RP, Garver JA, Edwards RH, and Kandler K (2010). Glutamate co-release at GABA/glycinergic synapses is crucial for the refinement of an inhibitory map. Nat. Neurosci 13, 232–238. [PubMed: 20081852]

Ruel J, Emery S, Nouvian R, Bersot T, Amilhon B, Van Rybroek JM, Rebillard G, Lenoir M, Eybalin M, Delprat B, et al. (2008). Impairment of SLC17A8 encoding vesicular glutamate transporter-3, VGLUT3, underlies nonsyndromic deafness DFNA25 and inner hair cell dysfunction in null mice. Am. J. Hum. Genet 83, 278–292. [PubMed: 18674745]

Rutherford MA, Chapochnikov NM, and Moser T (2012). Spike encoding of neurotransmitter release timing by spiral ganglion neurons of the cochlea. J. Neurosci 32, 4773–4789. [PubMed: 22492033]

Salvi RJ, Wang J, and Ding D (2000). Auditory plasticity and hyperactivity following cochlear damage. Hear. Res 147, 261–274. [PubMed: 10962190]

Schreiner C, and Winer JA (2005). The inferior colliculus (New York: Springer).

Seal RP, Akil O, Yi E, Weber CM, Grant L, Yoo J, Clause A, Kandler K, Noebels JL, Glowatzki E, et al. (2008). Sensorineural deafness and seizures in mice lacking vesicular glutamate transporter 3. Neuron 57, 263–275. [PubMed: 18215623]

Semple MN, and Kitzes LM (1985). Single-unit responses in the inferior colliculus: different consequences of contralateral and ipsilateral auditory stimulation. J. Neurophysiol 53, 1467–1482. [PubMed: 4009228]

Shepherd JD, Rumbaugh G, Wu J, Chowdhury S, Plath N, Kuhl D, Huganir RL, and Worley PF (2006). Arc/Arg3.1 mediates homeostatic synaptic scaling of AMPA receptors. Neuron 52, 475–484. [PubMed: 17088213]

Song X, Vizcarra C, Xu D, Rupert RL, Wong Z, Vizcarra C, Xu D, and Ru RL (2003). Hyperalgesia and neural excitability following injuries to central and peripheral branches of axons and somata of dorsal root ganglion neurons. J. Neurophysiol 89, 2185–2193. [PubMed: 12612043]

Sonntag M, Englitz B, Kopp-Scheinpflug C, and Rübsamen R (2009). Early postnatal development of spontaneous and acoustically evoked discharge activity of principal cells of the medial nucleus of the trapezoid body: an in vivo study in mice. J. Neurosci 29, 9510–9520. [PubMed: 19641114]

Spitzer NC (2006). Electrical activity in early neuronal development. Nature 444, 707–712. [PubMed: 17151658]

Stiebler I, Neulist R, Fichtel I, and Ehret G (1997). The auditory cortex of the house mouse: left-right differences, tonotopic organization and quantitative analysis of frequency representation. J. Comp. Physiol. A 181, 559–571. [PubMed: 9449817]

Sun S, Babola T, Pregernig G, So K, Nguyen M, Su M, Palermo A, Bergles DE, Burns JC, and Müller U (2018). Hair cell mechanotransduction regulates spontaneous activity and spiral ganglion subtype specification in the auditory system. Cell.

Syka J, and Popelá J (1984). Inferior colliculus in the rat: Neuronal responses to stimulation of the auditory cortex. Neurosci. Lett 51, 235–240. [PubMed: 6514239]

Tritsch NX, and Bergles DE (2010). Developmental regulation of spontaneous activity in the Mammalian cochlea. J. Neurosci 30, 1539–1550. [PubMed: 20107081]

Tritsch NX, Yi E, Gale JE, Glowatzki E, and Bergles DE (2007). The origin of spontaneous activity in the developing auditory system. Nature 450, 50–55. [PubMed: 17972875]

Tritsch NX, Zhang Y-X, Ellis-Davies G, and Bergles DE (2010a). ATP-induced morphological changes in supporting cells of the developing cochlea. Purinergic Signal. 6, 155–166. [PubMed: 20806009]

Tritsch NX, Rodríguez-Contreras A, Crins TTH, Wang HC, Borst JGG, and Bergles DE (2010b). Calcium action potentials in hair cells pattern auditory neuron activity before hearing onset. Nat. Neurosci 13, 1050–1052. [PubMed: 20676105]

Turrigiano GG, Leslie KR, Desai NS, Rutherford LC, and Nelson SB (1998). Activity-dependent scaling of quantal amplitude in neocortical neurons. Nature 391, 892–896. [PubMed: 9495341]

Wang HC, and Bergles DE (2014). Spontaneous activity in the developing auditory system. Cell Tissue Res.

Wang HC, Lin CC, Cheung R, Zhang-Hooks Y, Agarwal A, Ellis-Davies G, Rock J, and Bergles DE (2015). Spontaneous activity of cochlear hair cells triggered by fluid secretion mechanism in adjacent support cells. Cell 163, 1348–1359. [PubMed: 26627734]

Yan J, and Ehret G (2002). Corticofugal modulation of midbrain sound processing in the house mouse. Eur. J. Neurosci 16, 119–128. [PubMed: 12153536]

Yan J, and Suga N (1996). Corticofugal modulation of time-domain processing of biosonar information in bats. Science 273, 1100 LP–1103. [PubMed: 8688095]

Zhang-Hooks YX, Agarwal A, Mishina M, and Bergles DE (2016). NMDA receptors enhance spontaneous activity and promote neuronal survival in the developing cochlea. Neuron 89, 337–350. [PubMed: 26774161]
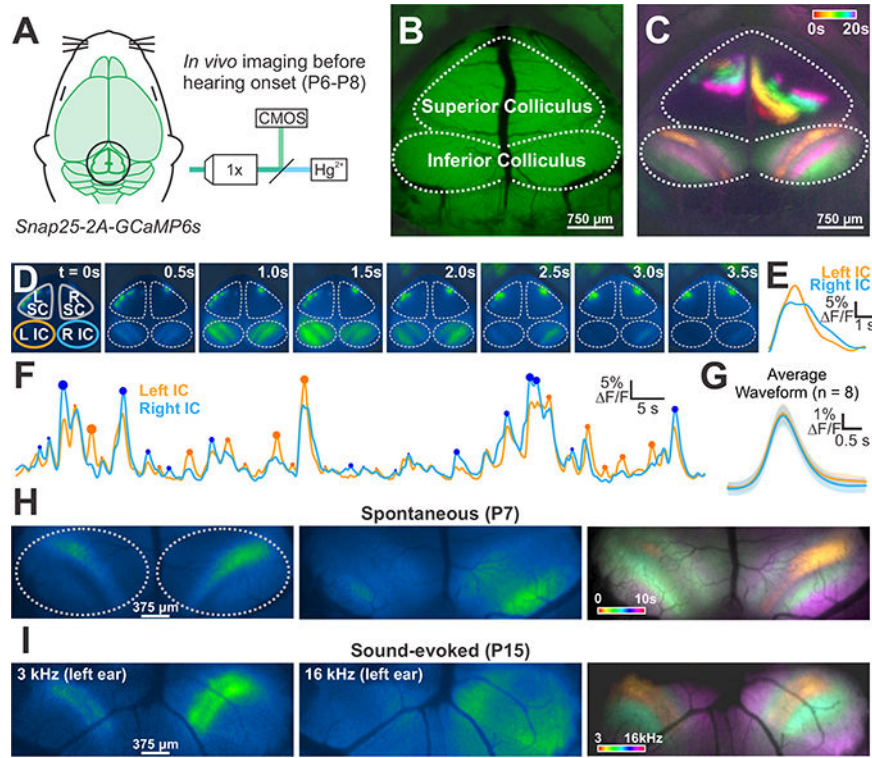
Figure 1. Imaging spontaneous neural activity in awake neonatal mice.

(A) Spontaneous neural activity monitored in unanesthetized mouse pups (*Snap25-T2A-GCaMP6s;* P6-P8) with wide field epifluorescence.

(B) Imaging field-of-view that includes the superior (visual) and inferior (auditory) colliculi (IC).

(C) Calcium transients in the midbrain color-coded based on time of occurrence.

(D) Time series of a discrete event in the IC.

(E) Fluorescence trace from time series in (D) of left (orange) and right (blue) IC.

(F) Fluorescence intensity over time for the two lobes of the IC. Circles highlight events that exhibit higher fluorescence compared to the contralateral lobe, and the size of the circle indicates the magnitude of difference between the two sides.

(G) Average waveform of all transients in left and right IC. Shaded area is S.E.M, n = 8 animals.

(H) Images of two spontaneous events before hearing onset. Image at right shows the spatial segregation of discrete events (color-coded based on time of occurrence), which were distributed throughout the IC.

(I) Tone-evoked neuronal calcium transients in P12 *Snap25-T2A-GCaMP6s* mice (after hearing onset). Image at right shows the tonotopic segregation of discrete events (color-coded based on sound frequency).
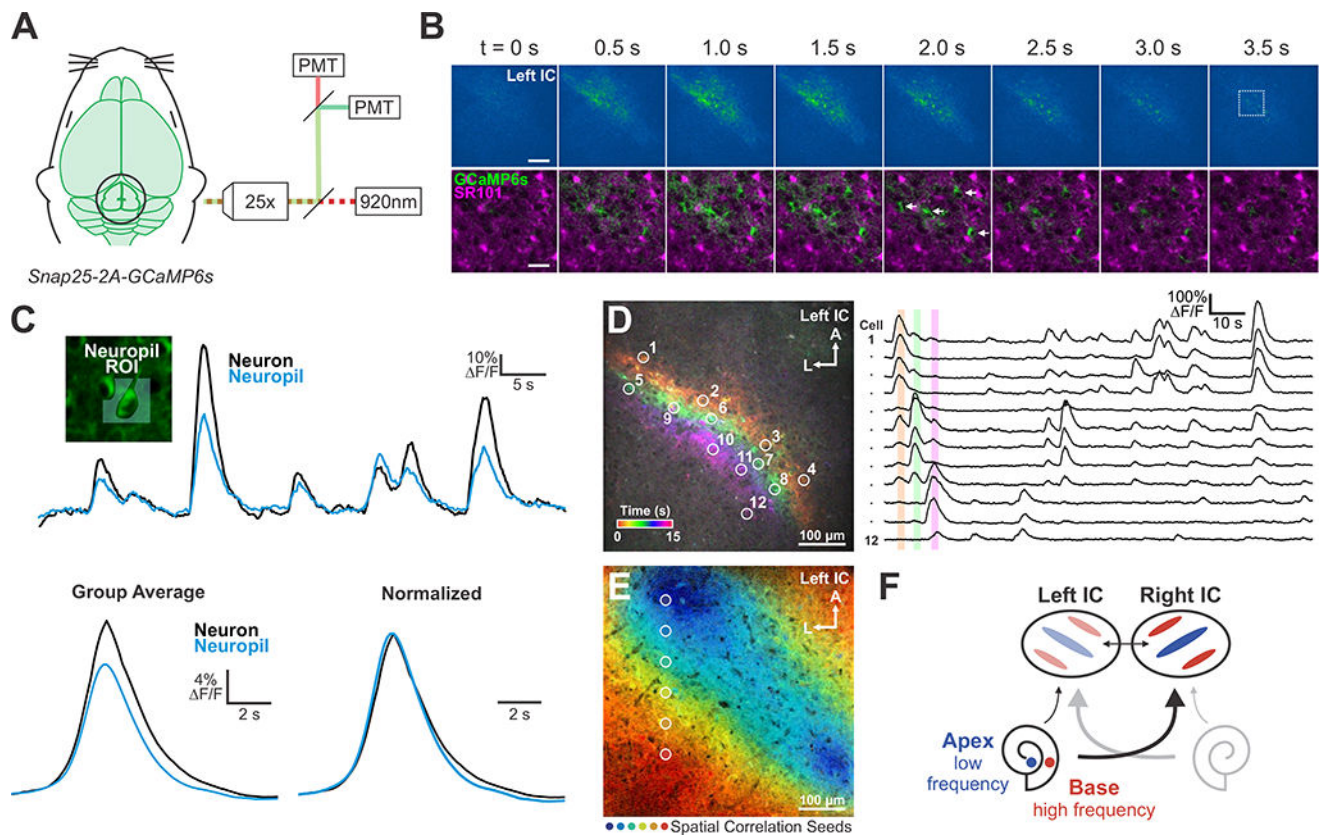
Figure 2. Spontaneous activity occurs in neurons and neuropil.

(A) Spontaneous neural activity monitored in unanesthetized mouse pups (P6-P8) using two-photon microscopy.

(B) Top: Time series of a representative spontaneous event recorded 150 μm below the pial surface. Scale bar = 100 μm. Bottom: Time series from box in top panel. SR101 was used to label astrocytes. Arrows indicate neuronal cell bodies. Scale bar = 25 μm.

(C) Fluorescence transients seen in neurons and adjacent neuropil (see Methods for details). Bottom: Group average of detected events. Fluorescence is normalized as F/F_o, where F_o is defined as the bottom 5th percentile of fluorescence values.

(D) Transients in the IC color-coded by time of occurrence. Right: Fluorescence traces from ROIs around individual neurons indicated on left.

(E) Spatial correlation map generated from seeds across the tonotopic axis; high spatial and temporal correlation indicated by color (see Methods for details).

(F) Model to explain how local activation of IHCs in the cochlea induces spatially restricted bands of neuronal activity in the IC.
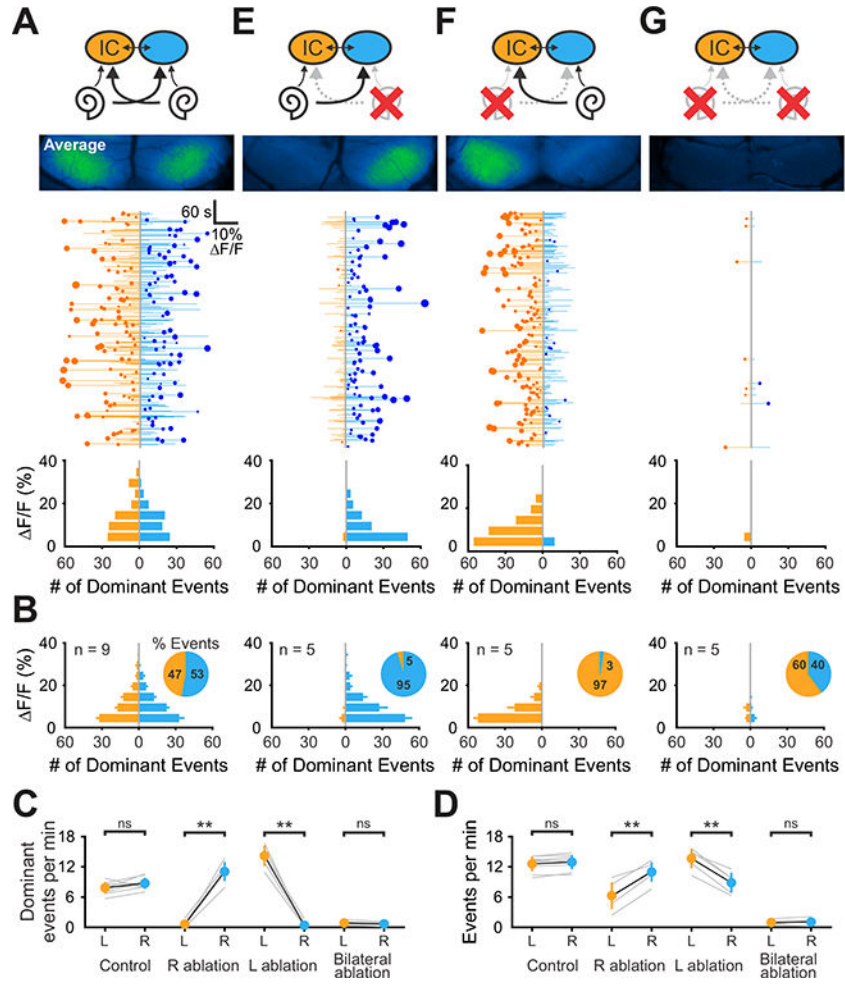
Figure 3. Spontaneous activity in the inferior colliculus originates in the cochlea.

(A) Top: Diagram illustrating flow of information through the auditory system and average intensity image over the 10-minute imaging session. Middle: Graph showing activity over time in left (orange) and right (blue) IC, where each line indicates the amplitude of the fluorescence change, the circle indicates the side which had the greatest intensity and the size of the circle indicates the difference in fluorescence. Bottom: Histogram showing the number of dominant events of different amplitudes.

(B) Average histogram of events across the group. Inset: pie graphs indicating the relative percentage of dominant events for each lobe.

(C) Graph of frequency of dominant activity in the left and right lobe of the IC across conditions. Gray lines indicate individual examples, black is the mean ± S.E.M. (n indicated in (**B**); two-tailed paired t-test, ns: not significant, **: $P < 0.005$).

(D) Graph of frequency of all activity in the left and right lobe of the IC across conditions. (n indicated in (**B**); two-tailed paired t-test, ns: not significant, **: $P < 0.005$).

(E - G) Similar to A, but for ablations of right, left, and both cochleae.
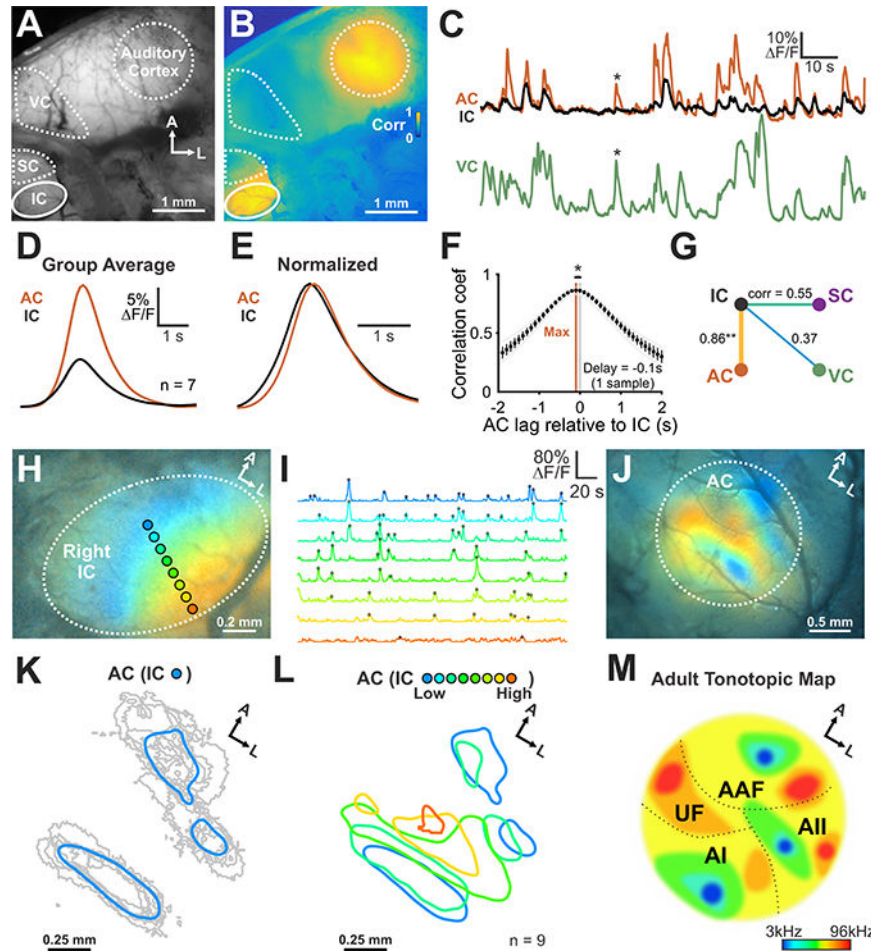
Figure 4. Auditory cortex receives tonotopically-organized information from inferior colliculus.
(A) Spontaneous neural activity across midbrain and cortex using wide field epifluorescence.

(B) Correlation map generated by performing a pixel-by-pixel correlation against signals from the IC (see Methods for details).

(C) Fluorescence transients seen in auditory cortex (AC), IC, and primary visual cortex (VC). Asterisk highlights cortical activity that was not correlated with IC activity.

(D) Average transient from IC and AC (n = 7 animals).

(E) Amplitude normalized transient from IC and AC (n = 7 animals).

(F) Cross-correlogram of signals in IC and AC. n = 7 animals (two-tailed paired Student's t-test, *: $P < 0.05$).

(G) Diagram displaying the average correlation coefficient between brain regions. (n = 7 animals; one-way ANOVA, Tukey's post-hoc, ** $P < 0.005$ for IC-AC versus all other correlations).

(H) Illustration of ROIs aligned to the future tonotopic axis of the IC. Colors in image indicate high correlations with the ROIs indicated.

(I) Normalized signals from ROIs indicated in (H). Detected peaks are indicated with filled circles.

(J) AC spatial activity map generated using activity from distinct zones within the IC. Concurrent activity in the IC and AC was averaged based on location of the peak within the IC. Each color corresponds to the ROIs indicated in (H).

(K) Individual (gray) and average area (blue) in the AC that exhibited correlated activity with future low frequency areas of the IC. Areas were defined by thresholding average response by 80% of maximum fluorescence.

(L) Group average spatial map in the AC generated from events within distinct, future tonotopic zones of the IC. Note that high frequency regions of the IC are underrepresented, due to the limited visualization of these deeper regions using wide field epifluorescence imaging.

(M) Schematic of AC organization in the adult mouse. AI: primary AC, AII: secondary AC, AAF: anterior auditory field, UF: ultrasonic field.
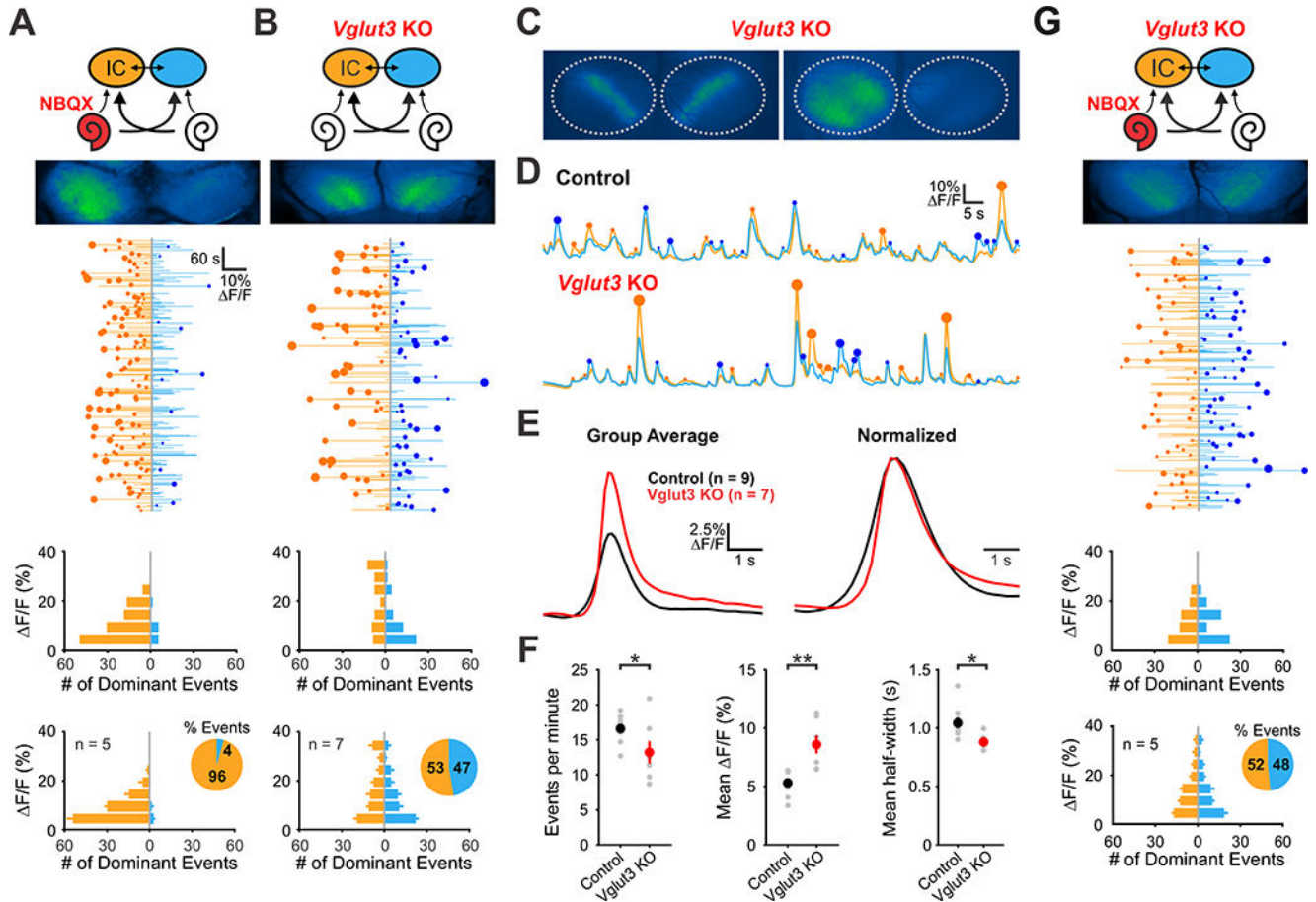
Figure 5. Spontaneous activity persists in mice lacking functional *VGLUT3*.

(A) Top: Diagram illustrating flow of information through the auditory system and average intensity image over the 10-minute imaging session. NBQX (50 mM) was applied to the left round window membrane. Middle: Activity over time in left and right IC in an individual where each line indicates the fluorescence intensity of each detected event, the circle indicates the dominant lobe, and the size of the circle indicated the difference in fluorescence. Bottom: Histograms showing the frequency of dominant events of a given amplitude for this experiment and for all experiments (n = 5 mice).

(B) Similar to A, but in *Vglut3* KO mice.

(C) Spontaneous events observed in *Vglut3* KO mice.

(D) Example fluorescence transients from control and *Vglut3* KO mice.

(E) Average and amplitude normalized transients from control and *Vglut3* KO mice.

(F) Comparisons of average frequency, amplitude, and half-width from control and *Vglut3* KO mice. (n = 9 control *(Snap25-T2A-GCaMP6s; Vglut3+/+)* and n = 7 *Vglut3* KO animals; twotailed paired Student's t-test with Bonferroni correction, *: $P < 0.05$, **: $P < 0.005$).

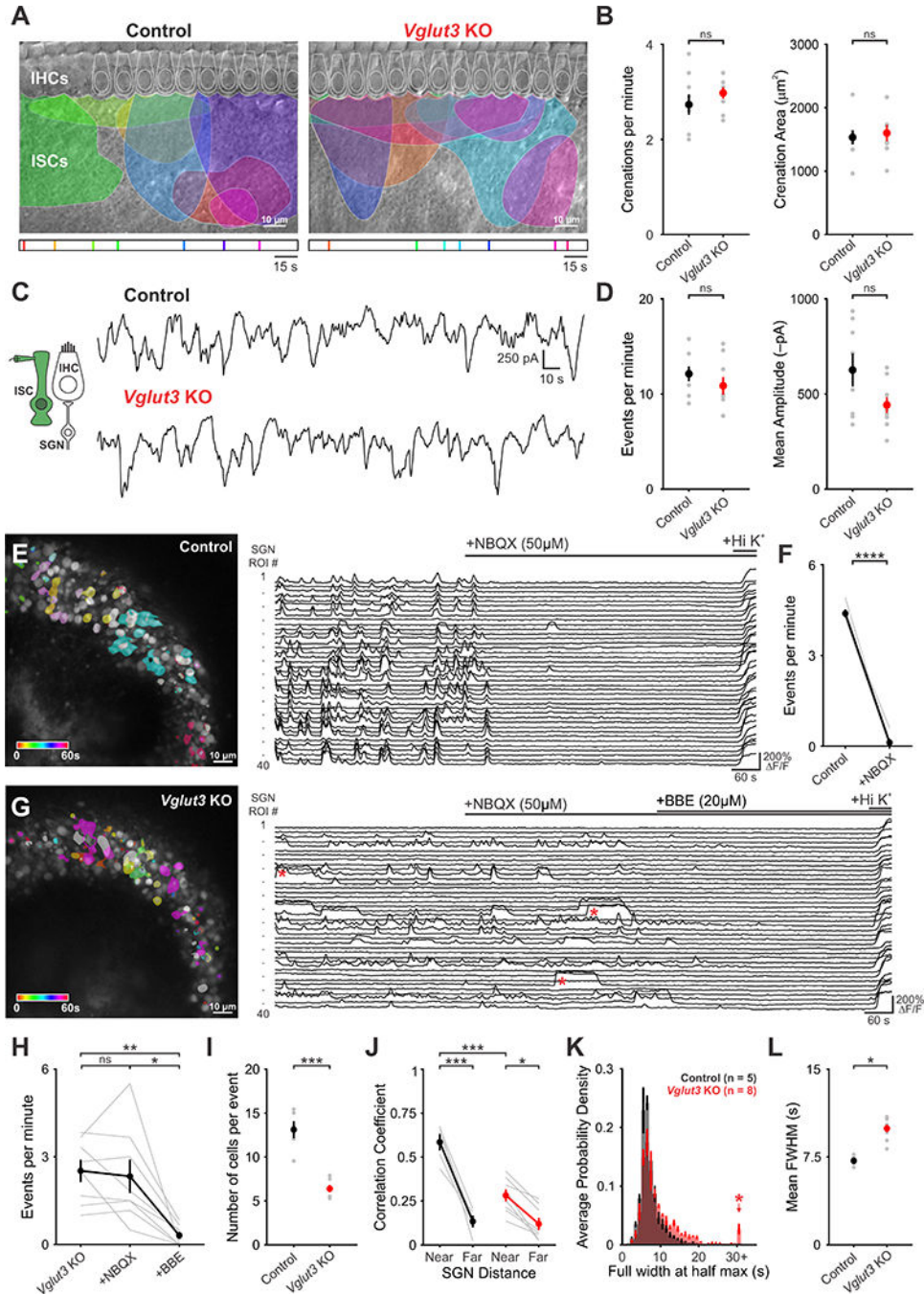(G) Similar to A, but in *Vglut3* KO mice with NBQX applied to the left ear.

Figure 6. Coordinated activation of spiral ganglion neurons by inner supporting cells persists in *Vglut3* KO mice.

(A) Intrinsic optical imaging performed in control and *Vglut3* KO mice. The maximum size of detected crenations are outlined by colors based on time of occurrence, as indicated bytimelines below images.

(B) Plots of crenation frequency and area. n = 7 cochlea from control and *Vglut3* KO mice (twotailed Student's t-test with Bonferroni correction applied, ns: not significant).

(C) Spontaneous inward currents recorded from inner supporting cells from (inset) from control and *Vglut3* KO mice.

(D) Plots of event frequency and event amplitude n = 8 cells from control and *Vglut3* KO cochlea (two-tailed Student's t-test with Bonferroni correction applied, ns: not significant).

(E) Time-lapse imaging of calcium transients from SGNs in *Snap25-T2A-GCaMP6s* mice (Left). Active cells are pseudocolored according to time of occurrence. Fluorescence traces from individual ROIs; bars indicate NBQX and high potassium application (Right).

(F) Quantification of event frequency before and after application of NBQX (50 μM). n = 5 cochlea (two-tailed paired Student's t-test, **** *P* < 0.0005).

(G) Time-lapse imaging of calcium transients in SGNs in the *Snap25-T2A-GCaMP6s;Vglut3* KO mice (Left). Active cells are pseudocolored according to time of occurrence. Fluorescence traces from individual ROIs; bars indicate NBQX, benzbromarone (BBE), and high potassium application (Right). Red asterisks highlight long duration, plateau calcium transients observed in *Vglut3* KO mice.

(H) Plot of event frequency before and after application of NBQX and BBE (n = 8 cochlea, oneway ANOVA, ns: not significant, * *P* < 0.05, ** *P* < 0.005).

(I) Plot of number of cells active during each event in control and *Vglut3* KO mice (n = 5 cochlea for control and n = 8 cochlea for *Vglut3* KO; two-tailed Student's t-test with Bonferroni correction, *** *P* < 0.0005).

(J) Plot of average correlation coefficient between the 5 nearest cells or the 5 farthest cells in control and *Vglut3* KO mice (n = 5 cochlea for control and n = 8 cochlea for *Vglut3* KO; twoway ANOVA with Tukey post hoc, *: *P* < 0.05, *** *P* < 0.0005).

(K) Probability density histograms of the duration (full width at half maximum, FWHM) of all events measured. Shown as mean ± S.E.M. Red asterisk highlights long duration events seen in *Vglut3* KO mice.

(L) Plot of mean duration of events (FWHM) (n = 5 cochlea for control and n = 8 cochleae for *Vglut3* KO; two-tailed Student's t-test, *: *P* < 0.05).
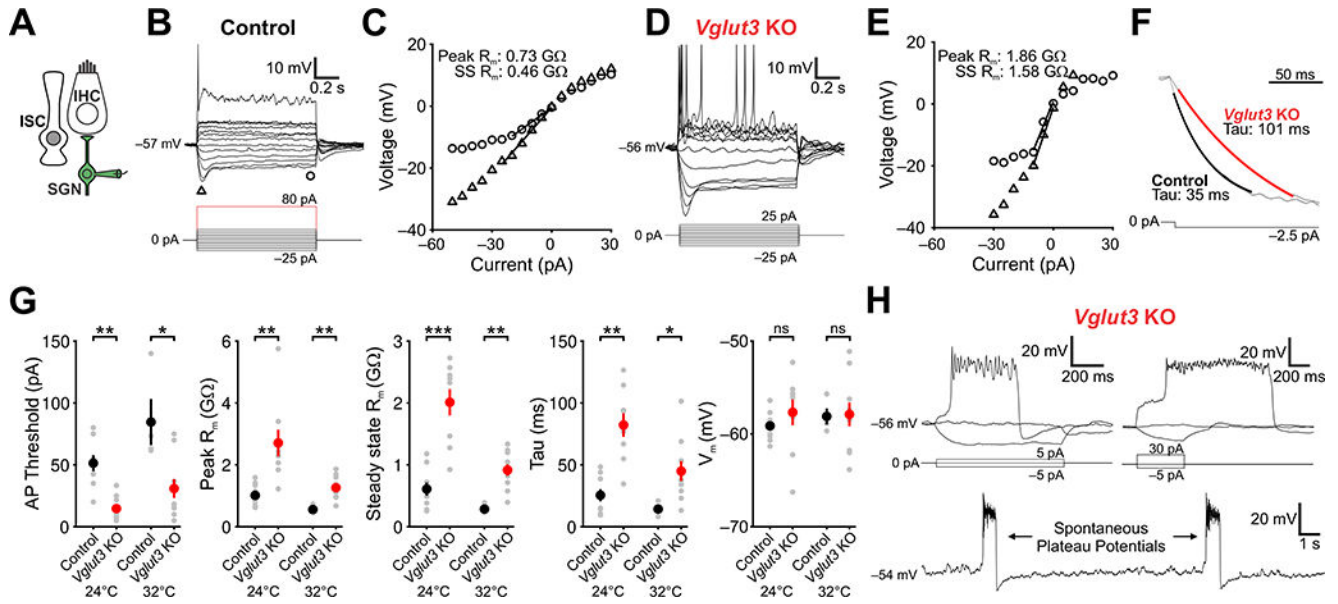
Figure 7. Spiral ganglion neurons in *Vglut3* KO mice exhibit enhanced excitability.

(A) Schematic of the whole-cell recording configuration.

(B) Membrane potential changes induced in an SGN from a control mouse in response to a series of current injections (indicated below) (−25 to 25 pA in 5 pA increments; first spike at 80 pA). Triangle and square indicate where the peak and steady-state voltage response were measured.

(C) I-V plot showing the membrane response to different current injections. Input resistance was obtained from the slope of the function between 0 and 20 mV (peak) and 0 to 15 mV (steady-state).

(D) Membrane potential changes induced in an SGN from a *Vglut3* KO mouse in response to a series of current injections (indicated below) (−25 to 25 pA in 5 pA increments; first spike at 15 pA).

(E) I-V plot showing the membrane response to different current injections. Input resistance was obtained from the slope between 0 and 20 mV (peak) and 0 to 15 mV (steady-state).

(F) Membrane potential response to −2.5 pA current steps in control and *Vglut3* KO mice. Tau measurements were obtained by fitting a single exponential between 10 and 90% max amplitude. Amplitudes were normalized.

(G) Plots of action potential threshold, peak and steady-state input resistance, tau, and resting membrane potential. For recordings at 24°C, n = 9 cells from 10 control cochleae and n = 8 cells from 6 *Vglut3* KO cochlea; for recordings at 32°C, n = 4 cells from 3 control cochleae and n = 11 from 6 *Vglut3* KO cochleae (two-tailed Student's t-test with Bonferroni correction, ns: not significant, *: $P < 0.05$, **: $P < 0.005$, ***: $P < 0.005$).

(H) Examples of plateau potentials evoked by current injection (top) and spontaneous plateau potentials observed at rest (bottom) in whole cell current clamp recordings from *Vglut3* KO mice. Note that the plateau potentials (top right) can outlast the stimulus.